Ignition and Flameholding in a Supersonic Combustor by an Electrical Discharge Combined with a Fuel Injector

K. V. Savelkin[1], D. A. Yarantsev[1], I. V. Adamovich[2], and S. B. Leonov[1,2]

[1]*Joint Institute for High Temperatures, Russian Academy of Sciences, 125412 Moscow, Russia*

[2]*Department of Mechanical and Aerospace Engineering, The Ohio State University, Columbus, OH, 43210, USA, leonov.2@osu.edu*

Abstract

The paper presents the results of an experimental study of supersonic combustor operation enhanced by an electrical discharge. A novel scheme of plasma assisted ignition and flameholding is demonstrated, which combines a wall fuel injector and a high-voltage electric discharge into a single module. The experimental combustor with the cross section of 72 mm (width) × 60 mm (height) and length of 600 mm operates at a Mach number of M=2, initial stagnation temperature of airflow of T_0=290-300 K, and stagnation pressure of P_0 = 1.3 – 2.0 Bar. The combustor is equipped with four plasma ignition modules, flush-mounted side-by-side on the plane wall of the combustion chamber. The combustion tests were performed using ethylene injection with a total mass flow rate of $G_{C2H4} < 10$ g/s and discharge power in the range of W_{pl} = 3 – 24 kW. The scope of the experiments includes characterization of the discharge interacting with the main flow and fuel injection jet, parametric study of ignition and flame front dynamics, and comparison of the present scheme to previously tested configuration. The present approach demonstrates a significant advantage in terms of flameholding limits. An operation mode with strong combustion oscillations was observed at high fuel injection flow rates. Methods of flame front stabilization based on plasma application are discussed. The technique studied in the present work has significant potential for high-speed combustion applications, including cold start / restart of scramjet engines and support of transition regime in dual-mode and off-design operation.

Report Documentation Page

Form Approved
OMB No. 0704-0188

1. REPORT DATE	2. REPORT TYPE	3. DATES COVERED
2014		**00-00-2014 to 00-00-2014**

4. TITLE AND SUBTITLE	5a. CONTRACT NUMBER
Ignition and Flameholding in a Supersonic Combustor by an Electrical Discharge Combined with a Fuel Injector	5b. GRANT NUMBER
	5c. PROGRAM ELEMENT NUMBER
6. AUTHOR(S)	5d. PROJECT NUMBER
	5e. TASK NUMBER
	5f. WORK UNIT NUMBER
7. PERFORMING ORGANIZATION NAME(S) AND ADDRESS(ES) **Ohio State University,Department of Mechanical and Aerospace Engineering,201 W. 19th Ave,Columbus,OH,43210**	8. PERFORMING ORGANIZATION REPORT NUMBER
9. SPONSORING/MONITORING AGENCY NAME(S) AND ADDRESS(ES)	10. SPONSOR/MONITOR'S ACRONYM(S)
	11. SPONSOR/MONITOR'S REPORT NUMBER(S)

12. DISTRIBUTION/AVAILABILITY STATEMENT
Approved for public release; distribution unlimited

13. SUPPLEMENTARY NOTES
accepted for publication in Combustion and Flame, 2014.

14. ABSTRACT

The paper presents the results of an experimental study of supersonic combustor operation enhanced by an electrical discharge. A novel scheme of plasma assisted ignition and flameholding is demonstrated, which combines a wall fuel injector and a high-voltage electric discharge into a single module. The experimental combustor with the cross section of 72 mm (width)  60 mm (height) and length of 600 mm operates at a Mach number of M=2, initial stagnation temperature of airflow of T0=290-300 K, and stagnation pressure of P0 = 1.3 ? 2.0 Bar. The combustor is equipped with four plasma ignition modules, flush-mounted side-by-side on the plane wall of the combustion chamber. The combustion tests were performed using ethylene injection with a total mass flow rate of GC2H4 < 10 g/s and discharge power in the range of Wpl = 3 ? 24 kW. The scope of the experiments includes characterization of the discharge interacting with the main flow and fuel injection jet, parametric study of ignition and flame front dynamics, and comparison of the present scheme to previously tested configuration. The present approach demonstrates a significant advantage in terms of flameholding limits. An operation mode with strong combustion oscillations was observed at high fuel injection flow rates. Methods of flame front stabilization based on plasma application are discussed. The technique studied in the present work has significant potential for high-speed combustion applications, including cold start / restart of scramjet engines and support of transition regime in dual-mode and off-design operation.

15. SUBJECT TERMS

16. SECURITY CLASSIFICATION OF:			17. LIMITATION OF ABSTRACT	18. NUMBER OF PAGES	19a. NAME OF RESPONSIBLE PERSON
a. REPORT	b. ABSTRACT	c. THIS PAGE			
unclassified	**unclassified**	**unclassified**	**Same as Report (SAR)**	**24**	

1. Introduction

Compared to a basic scramjet design, operation of scramjet combustors using plasma assisted ignition and flameholding offers considerably more flexibility over the choice of its geometry, due to replacing mechanical flameholders with a highly effective electrically driven apparatus. Over the years, many studies have been conducted to develop an alternative plasma-based ignition system that could consistently and reliably ignite non-stoichiometric mixtures over a wide range of pressures and temperatures [1-3]. Plasma technologies, such as plasma torches, plasma rails, and others, rely on high energy density electrical discharges to produce ionization and initiate combustion due to thermal / chemical activation of fuel or fuel / air mixtures [3-4]. A number of experimental studies have been performed at conditions typical for scramjet operation [5-9]. In most of these experiments, a modification of supersonic duct geometry was used, such as a backward facing wall step or a contoured cavity, and plasma was employed as an igniter of a combustible mixture in a low-speed flow region. At the same time, some of previous experiments using an alternative configuration, where an electric discharge was sustained over a plane wall [10-11], demonstrated feasibility of plasma application as an effective igniter and flameholder in a supersonic combustor, without relying on mechanical obstacles for flameholding.

Another aspect of the problem is the effect of highly non-equilibrium chemical kinetics, which may help reducing the plasma power needed for reliable ignition by enhancing specific chemical reactions pathways. Significant progress in this field has been made over the last 15 years [3, 4, 12-15]. Dramatic reduction of ignition time has been demonstrated, up to several orders of magnitude at premixed conditions, over a range of stagnation temperatures specifically important for scramjet technology, T_0 = 500-900 K. In spite of these promising results, this approach appears to be rather impractical for high-speed flow engines with direct fuel injection. In most cases, the main limiting factor is rather slow fuel-air mixing, resulting in strong gradients of fuel/oxidizer ratio across the combustion chamber. The most challenging issue in this case is to determine the most effective location of the electric discharge plasma, which is typically non-uniform, in a shear layer between the fuel injection jet and the main airflow.

In this work, a novel pattern of plasma-fuel interaction is studied experimentally. In the present method, an electric discharge is located partially inside the fuel injection orifice, chemically preprocessing (i.e. partially reforming) the fuel prior to injection and accelerating mixing by introducing strong thermal inhomogeneity into the flowfield. This approach employs the following three critically important physical effects: (1) fast ionization wave propagating predominantly along solid surfaces (such as walls of delivery lines) and gas flows [16-17]; (2) penetration of discharge current into the main airflow, following a fuel injection jet [18]; and (3) discharge localization within the shear / mixing layer between two components of the mixture [19]. The first effect causes near-surface ionization wave propagation along gas delivery lines during high-voltage breakdown, over long distances, resulting in significant reduction of breakdown voltage over long gaps between the electrodes. After breakdown, the electric current follows the injection jet flow, due to convective transport of the plasma and lower density in the

jet. Finally, the axial part of the plasma filament is localized inside the fuel-air mixing layer.

The present paper is focused on an experimental study of hydrocarbon fuel ignition and flameholding in a novel configuration of the plasma / injection module. The experimental data obtained using the new plasma-injection module (PIM) are compared to previously tested schemes, where the plasma is generated in airflow in front of the fuel injection port [10, 11]. This type of PIM has a significant potential for mixing enhancement and flameholding in supersonic combustors.

2. Experimental apparatus

The experiments were performed in a supersonic blow-down wind tunnel PWT-50H [10-11], the schematic of which is shown in Fig. 1a. In the present configuration, the test section operates as a supersonic combustor, with the PIM for ethylene ignition and flameholding flush-mounted on a plane wall, as shown in Fig. 1b. The combustor cross section is Y × Z = 72 mm (width) × 60 mm (height), with the length of X = 600 mm. It is furnished with three pairs of circular high-quality quartz windows, providing ample optical access. To avoid thermal chocking during fuel ignition, the test section has a 10° expansion angle downstream of the PIMs on the opposite (bottom) wall, to the cross section of Y × Z =72 mm (width) × 72 mm (height). The experimental conditions are as follows: initial Mach number M=2; static pressure P_{st} = 160-250 Torr; air mass flow rate G_{air} = 0.6-0.9 kg/s; ethylene mass flow rate G_{C2H4}= 1-8 g/s; duration of steady-state aerodynamic operation ~ 0.5 s.

The test section of PWT-50H high-speed combustion facility is equipped by 3 pairs of 100 mm diameters windows placed in the side walls of the duct for optical access. The first pair of windows is located near the upstream side of the combustor and provides optical access to the area where PIM modules are installed. The second pair of windows is placed downstream, with a 65 mm gap between the two pairs of windows. The third pair of windows is typically used for TDLAS measurements, as has been done in our previous work [20]. Instrumentation includes the pressure measuring system, the schlieren system, UV/visible optical emission spectrometer, current and voltage sensors, Tunable Diode Laser Absorption Spectroscopy (TDLAS) apparatus for water vapor concentration measurements, 5-component exhaust flow chemical analyzer, high-speed cameras, and operation sensors.

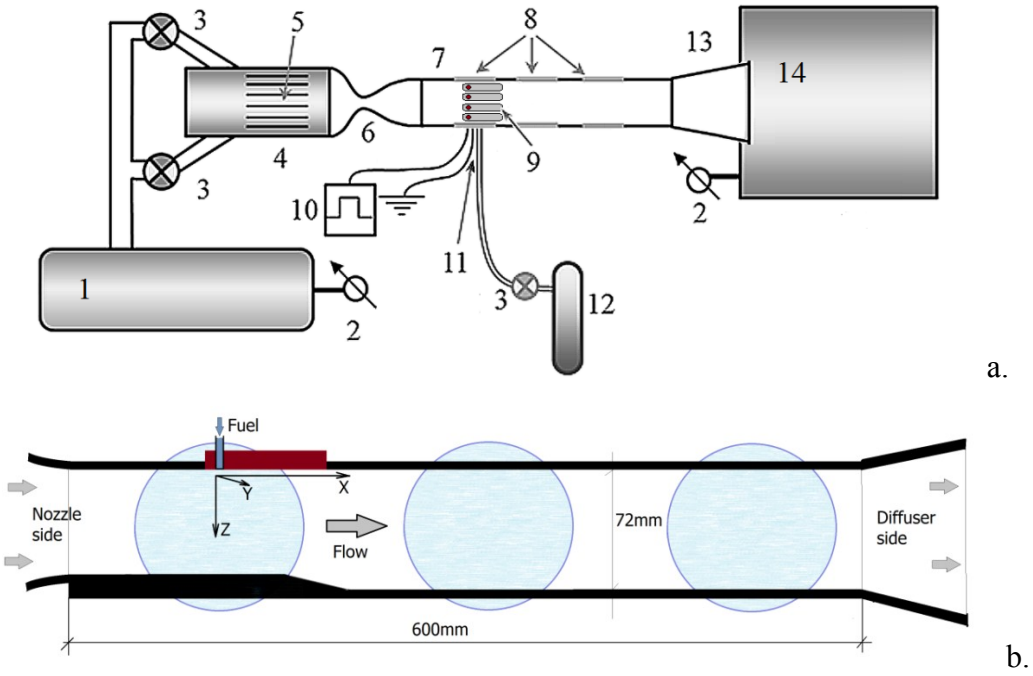

Figure 1. Schematic of experimental facility PWT-50H. (a) General layout: 1 – high pressure tank; 2 – operation gauges; 3 – solenoid valves; 4 – plenum section; 5 – honeycomb; 6 – nozzle; 7 – test section; 8 – optical access windows; 9 – plasma-injector modules; 10 – high-voltage power supply; 11 – fuel ports / discharge connectors; 12 – fuel tank; 13 – diffuser; 14 – low-pressure tank. (b) Test section wall profile: optical windows are indicated by circles, location of plasma injection modules (PIM) is shown by a rectangle in the top wall of the test section.

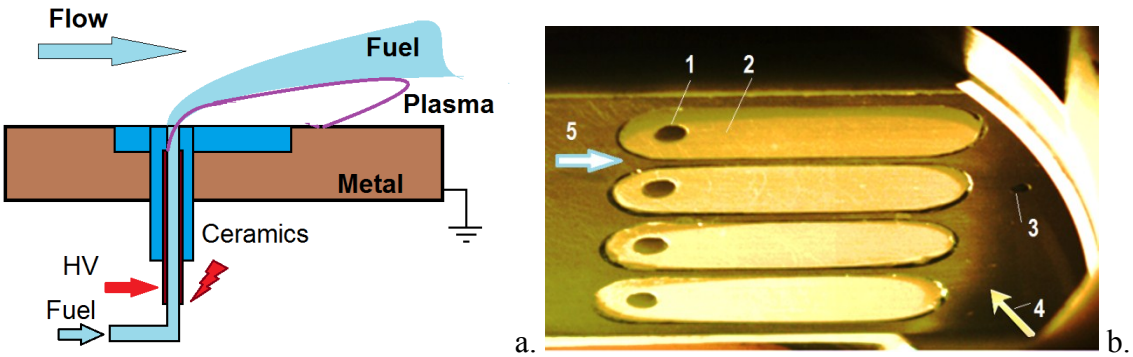

Figure 2. (a) Schematic of electrodes and fuel injectors in a single PIM. High-voltage discharge initiates from the high-voltage electrode inside the fuel injector line, propagates along the fuel injection jet, and terminates at the grounded metal wall of the combustor. (b) Photograph of a row of PIMs in the test section: 1- fuel injection orifice, 2- ceramic insert, 3- pressure tap, 4- direction of view, 5- flow direction.

The schematic of a single PIM module is shown in Fig. 2(a). The high-voltage electrode (anode) is integrated into the fuel injector. For this, a metal tube is inserted into a ceramic injection orifice. The distance between the end of the tube and the duct wall surface, $Z1 \leq 10$ mm, is sufficiently long to ensure significant impact of the discharge on the fuel flow prior to its injection into the main airflow. The fuel is injected into the main flow through circular orifices d=4 mm in diameter. In the present experiments, four PIMs are inserted into the top wall of the test section, arranged side-by-side spanwise, as shown in Fig. 2(b). The fuel mass flow rate is evenly distributed between the injection orifices using the fuel plenum. The duration of the discharge operation was in the range of 100-150 ms, typically 100 ms. Fuel injection was started about 20 ms after the discharge initiation and stopped before the discharge was turned off. In some runs, fuel injection continued 10-20 ms after the discharge to detect whether the flame was maintained or extinguished. In each operation mode, fuel was injected through all four orifices. In contrast to previously tested experimental configurations [11], the present scheme allows using a metal combustion chamber.

Four discharge operation modes have been tested:

- Mode A: all four electrodes are powered, #1, #2, #3, and #4;
- Mode B: two central electrodes are powered, #2 and #3;
- Mode C: two lateral electrodes are powered, #1 and #4;
- Mode D: only one electrode is powered, #2.

The custom-made power supply used in the present experiments is designed to operate with a steep falling voltage-current characteristic and individual control of each output channel. Control of output power is performed by varying the internal resistance of the power supply. At typical experimental conditions, the power supply operates in nearly current-stabilized mode. Voltage across the gap and discharge current are measured by Tektronix P6015A high-voltage probe and Agilent 1146A current probe during the run for each module, which allows calculating discharge power coupled to the individual PIM.

The facility is equipped with the static pressure scanner NetScanner 9116 with 16 static pressure sensors, B1 - B16, at the following axial locations relative to the fuel injector port, X= -82, -18, -8, 20, 50, 60, 105, 130, 155, 180, 230, 280, 330, and 160 mm on the bottom wall, stagnation pressure sensor P_{Pitot}, pressure in vacuum tank P_{lp}. Schlieren visualization was used as the main tool to study dynamics of the flow structure modification during fuel ignition induced by the plasma. The high resolution schlieren system uses a high-power pulsed diode laser (pulse duration t_{exp}=100 ns) and a framing camera (frame rate up to 1000 frames per second, Basler A504K). Emission spectra of the plasma luminescence were recorded by the Lot-ORIEL spectrometer with Andor CCD camera. The spectral dispersion is 0.035 nm/pixel, and the spectral resolution is $\Delta\lambda \sim 0.13$ nm. The spectroscopic system collects plasma emission from a cylindrical volume aligned in the Y direction from window to window and with diameter of 10 mm. During the operation, the spectrometer takes an emission spectrum each 10 ms.

3. Discharge characterization

Typical photographs of the discharge, taken during operation in Mode A, without and with fuel injection, are presented in Fig. 3. Total discharge power in this mode was W_{pl} = 6-24 kW. Both discharge voltage and current were oscillating because of variation of discharge filament lengths, within a range of U_{pl}=0.7-2 kV and I_{pl}=2-7 A, respectively. Prior to fuel injection, the discharge power was distributed equally between the modules. After injection, discharge power increased for the two centrally located PIMs and decreased for the two lateral modules.

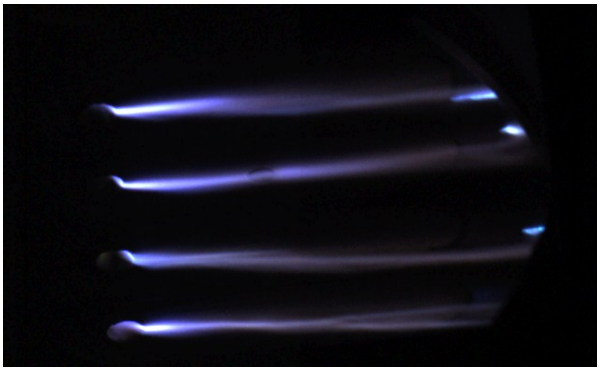
a.
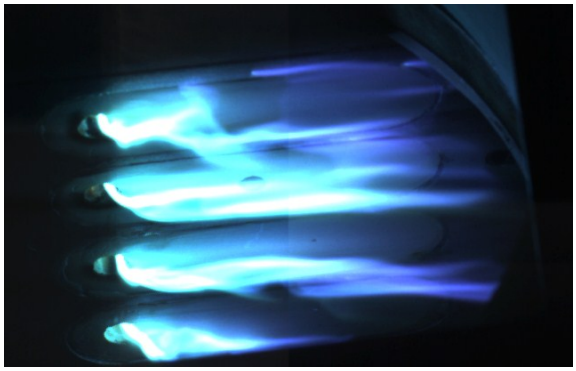
b.

Figure 3. Photographs of electrical discharge in combustion chamber, exposure time of t=100 μs (compare to Fig. 2b for details): a – no ethylene injection, total discharge power W_{pl}=12 kW; b – during ethylene injection, mass flow rate G_{C2H4}=2 g/s, total discharge power W_{pl}=14 kW.

In the beginning of plasma filament development, breakdown occurs along the path inside the injector and a short gap between the injection orifice and a grounded metal wall upstream of the injector. After this, the filaments are convected by the flow downstream of the injector, terminating to the grounded wall downstream of the ceramic inserts, shown in Fig. 2. After this occurs, the plasma filaments extend downstream over a distance up to 100 mm, close to the surface of the ceramic insert. The location of filament termination at the grounded wall oscillates at a frequency of F=10-20 kHz. The filament behavior changes significantly after fuel injection. Specifically, plasma emission intensity increase and the plasma filaments move away from the surface.

Typical dynamics of time-resolved discharge power for 4 individual modules is shown in Fig. 4(a). In spite of large magnitude of high-frequency oscillations, the time-averaged power values are quite stable and repeatable from run to run. It is also seen that the value of the discharge power varies during the run. Fuel injection and ignition lead to the increase of the discharge power in the central modules, due to significant extension of the length of plasma filaments and the resultant rise of gap voltage, as shown in Fig. 4(b). At a certain value of fuel

injection flow rate, intense heat release in chemical reactions in the near-centerline zone of the combustor induces flow separation near the duct corners, which consequently reduces the length of the lateral plasma filaments, as well as the discharge power in the lateral modules. These processes are illustrated in Fig. 5, where the discharge photographs are shows for two different values of the fuel injection flow rate, one without flow separation in the corners (Fig. 5(a)) and the other with flow separation (Fig. 5(b)). No separation was detected in mode C, when only the two lateral discharge modules were powered.

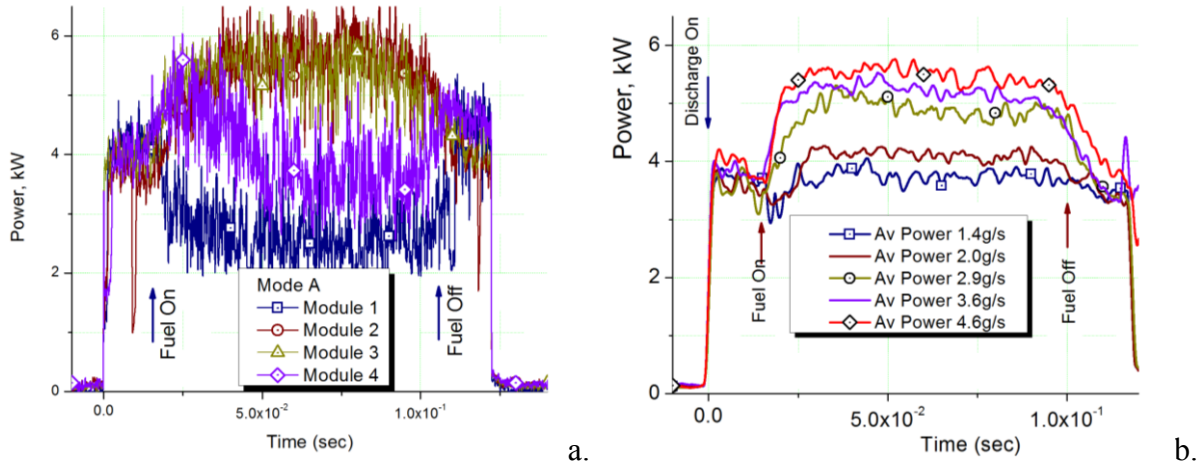

a. b.

Figure 4. (a) Discharge power dynamics and distribution among the PIM modules in Mode A (all modules powered), calculated from voltage and current measurements. G_{C2H4}=3 g/s, averaged current I_{pl}=4A. (b) Discharge power in module #3 vs. fuel injection flow rate. Low-pass filter is applied to reduce high-frequency oscillations.

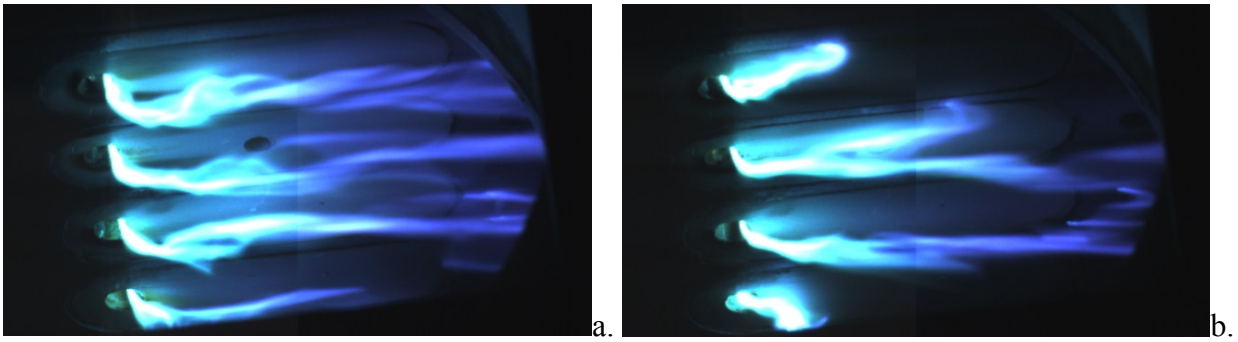

a. b.

Figure 5. Photographs of discharge filaments during combustion, exposure time of t=100 μs: (a) G_{C2H4}=2g/s, no flow separation near the side walls; (b) G_{C2H4}=3.6 g/s, flow is separated near the side walls. Flow direction is from left to right.

The discharge power can be regulated approximately by varying the average output current of the power supply, as shown in Fig. 6(a). It should be noted that the power deposition is not proportional to the average discharge current because increasing the current somewhat reduces the gap voltage. Operation characteristics of individual PIM modules depend to some extent on whether the adjacent modules are powered or not, especially for the lateral modules. Typical distribution of power among the modules is shown in Fig. 6(b), for all four operation modes tested (A-D).

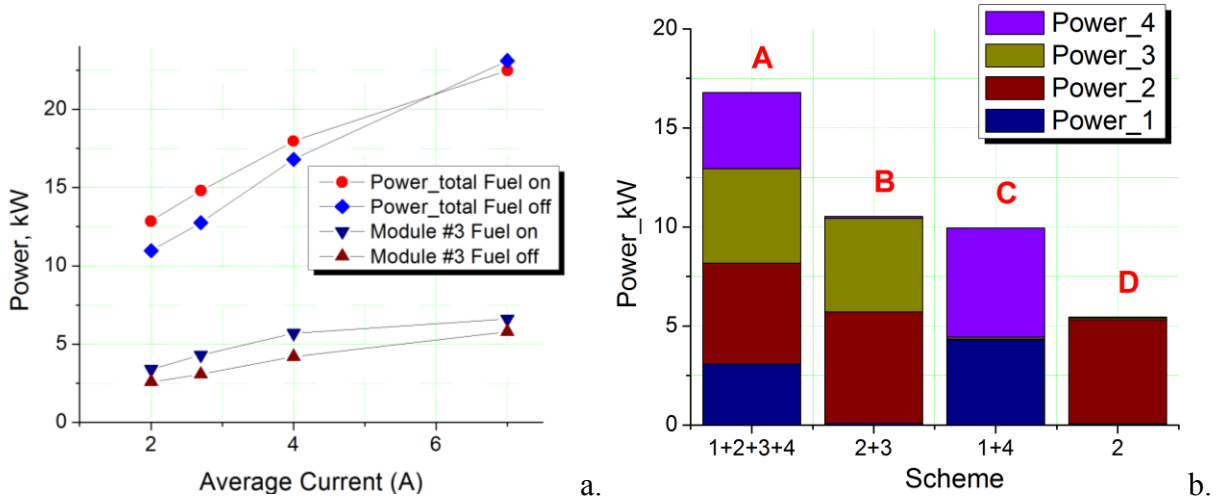

Figure 6. (a) Discharge power vs. time-averaged power supply current, for all four modules and for a single module. G_{C2H4}=3g/s, operation in Mode A. (b) Diagram of power distribution among the modules for different operation modes. G_{C2H4}=3g/s, time-averaged current I_{pl}=4A.

A composite optical emission spectrum of the plasma, taken by integrating the emission from the area of plasma-fuel-flow interaction, X=20-30mm, Y=0-10 mm, is displayed in Fig. 7. Analysis of the spectra shows that in the presence of the hydrocarbon fuel, three different types of species are detected: hydrocarbon/carbon fragments, chemical reaction products resulting from interaction of hydrocarbon plasma and air, and excited air species (mainly N_2). Species with highest emission intensity include atomic hydrogen, carbon and oxygen (O atom triplet line at λ=777 nm outside of the spectral range of Fig. 7), hydrogen molecule H_2, as well as C_2, CN, OH and CH radicals. Neglecting continuum emission, the molecular bands of CN radical violet system, CN ($B^2\Sigma \rightarrow X^2\Sigma$), and C_2 Swan bands contribute up to 50% of integrated emission intensity. These spectra indicate intense chemical transformations in the flow, including generation of active radicals in electronically excited states.

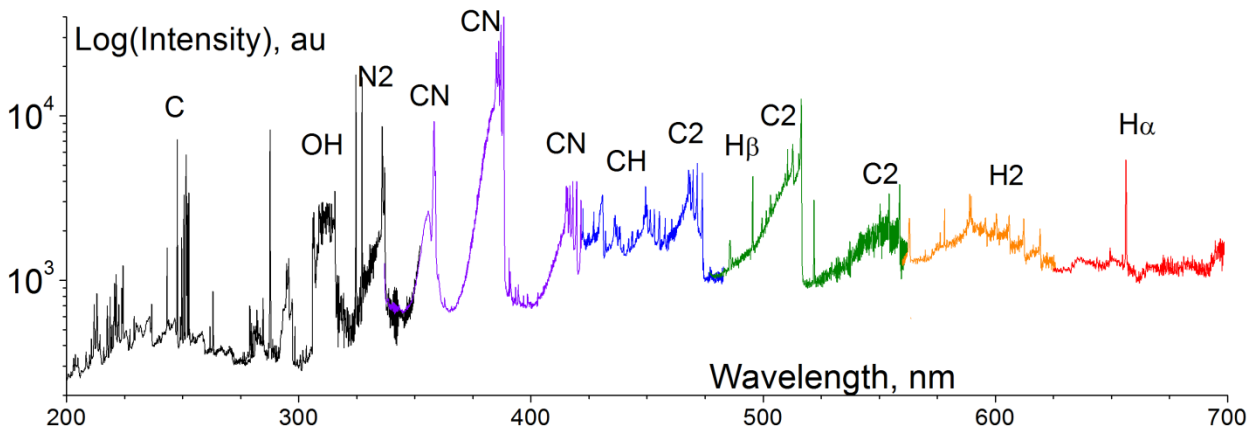

Figure 7. Composite optical emission spectrum taken from the ethylene-airflow-plasma interaction region. The spectrum incorporates seven overlapping spectra, taken separately at the same conditions. Mode A, discharge current I_{pl}=2-4A, ethylene injection jet G_{C2H4}=0.5-1 g/s from each module in M=2 airflow, P_{st}=180-220 Torr. Major emission lines and bands are labeled.

The emission spectra were used to evaluate plasma parameters in a zone near the base of the fuel injection jet. Second positive system of molecular nitrogen, N_2 ($C^3\Pi_u$,v′=0 → $B^3\Pi_g$,v″=0) band at λ=337.1 nm was employed to infer the rotational-translational temperature in the plasma [21], T_r= 3000 ± 500 K, which is strongly weighted toward the peak temperature in the plasma filament. The H atom Balmer series lines are very intense, with the H_α line at λ=656.3 nm being the strongest in this case. Electron density in the plasma was extracted from H_α spectral line shape [22, 23], since Stark effect is the dominant mechanism of line broadening at the present conditions. Electron density near the base of the fuel injection jet is inferred to be n_e= $(4.5\pm1.0)\cdot10^{15}$ cm^{-3}.

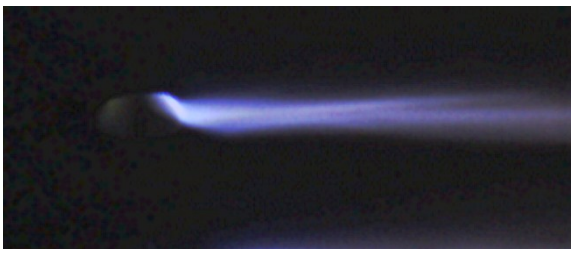
a.
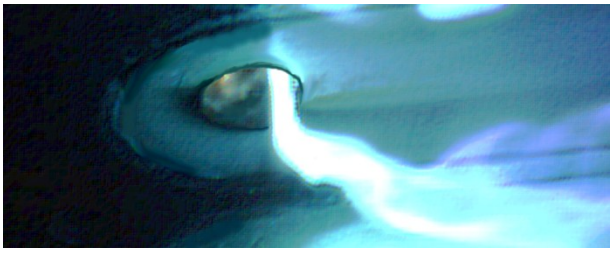
b.

Figure 8. Photographs of the part of the discharge filament in the flow near the injection orifice, (a) without fuel injection, and (b) with ethylene injection. In the second case, the electric current follows the injection jet. Orifice diameter d=4 mm.

The mechanism of plasma interaction with a jet of fuel injected into the airflow is of major importance for dynamics of ignition and flameholding at the present conditions. From

comparison of images in Fig. 8a and Fig. 8b, it is apparent that plasma emission, which serves as an indicator of energy loading by the discharge (i.e. indicating the presence of both electric field and discharge current), essentially follows the fuel jet. The effect of electrical current convecting with the flow has been previously observed in a near-surface transverse filament discharge between two pin electrodes in Mach 2 airflow [24]. In Mach 2.8 airflow, near-surface transverse DC discharge filament between two electrodes extended in the flow direction convected in the boundary layer at a velocity of approximately 60% of free stream velocity [25].

Quantitative prediction of the discharge behavior in the fuel injection flow at the present conditions can be obtained using a plasma fluid model, incorporating equations for electron and ion densities and the Poisson equation for the electric field, as discussed in detail in the Appendix. Quantitatively, the filament shape and discharge current path through the fuel injection jet, reacting mixing layer, and the air flow is controlled by trade-off between at least two factors, (i) maximum value of the effective ionization coefficient, i.e. the difference between ionization and attachment coefficients, $\alpha(E/N) - \eta(E/N)$, and (ii) maximum effect of convection by the flow. Note that the ionization coefficient depends not only on the electric field but also on temperature and mixture composition, which are controlled by Joule heat in the discharge, electron impact fuel dissociation in the jet (with most dominant products being C_2H_3 C_2H_2, H_2, and H atoms [26]), oxygen fraction in the mixing layer, and heat release due to fuel oxidation reactions.

4. Experimental results on ignition and flameholding

A series of experiments was performed on ethylene ignition and flameholding by means of the electrical discharge collocated to the fuel injection jet, described in Section 3. The following test parameters have been varied: (1) fuel injection flow rate, within a range of G_{C2H4} = 1 – 8 g/s; (2) discharge time-averaged current (i.e. discharge power); and (3) discharge operation mode, from A to D (see Section 2). First of all, it has been determined that ignition and flameholding are observed over a much wider range of parameters compared to previously tested configurations, both with upstream and downstream location of the electric discharge relative to fuel injection port [11, 27].

4.1. Plasma-assisted combustion: effect of fuel mass flowrate and discharge power.

Typical schlieren images are shown in Fig. 9(a), illustrating the baseline flow structure before fuel injection, and in Fig. 9(b), during combustion. These composite images are assembled from two images taken during different runs with similar operating parameters. The location of the PIM row is indicated in Fig. 9(b). When the discharge is turned on, the location of the plasma filament near the injection orifice becomes visible because of oblique shock generation. The oblique shock wave interacts with an expansion wave generated by angle step expansion of the bottom test section wall (see Fig. 9(b)), and then with a compression wave

generated there when the flow velocity vector is reversed. When the flame front is stabilized (during steady-state flameholding), the combustion process appears to progress slowly in the axial direction, due to gradual mixing of fuel and air. Chemical energy release during combustion elevates the pressure and forms a wedge-shape combustion zone, with its average angle increasing as combustion intensifies. The attached oblique shock wave angle increases accordingly. Flow separation near the side wall at the PIM location is also evident in Fig. 9(b). Further increase of fuel mass flow rate would result in separation zone moving upstream, thus increasing the oblique shock wave angle, and eventually leading to thermal chocking of the duct.

The other side of electrical discharge effect on combustion is enhancement of air-fuel mixing in high-speed flows. Both direct and indirect mechanisms of plasma-flow interaction are responsible for this effect. First, plasma-based heating generated in the flow acts as a "gradual" obstacle, generating a vortex flow similar to a Karman vortex trail. An additional, direct, plasma effect is caused by strong modulation of power deposition in the electric discharge, which results, depending of the discharge location, in boundary or shear layer tripping. As seen in Fig. 4a, modulation of instantaneous discharge power is up to ~50% of the average power value; the frequency of the modulation is 10-20 kHz. An indirect mechanism of mixing enhancement is realized through the Richtmyer-Meshkov instability, appearing in flows with non-collinear gradients of density and pressure. This leads to formation of deterministic vortex-dominated and, subsequently, small-scale stochastic perturbations resulting in turbulent mixing [28]. Two regions of the flow field, labeles as A and B in Fig. 9b, are of particular interest. In region A, shock waves caused by the test section walls imperfections and originating upstream of the field of fiew interact with the fuel jet with a high density gradient, caused by plasma-induced non-uniform heating. In region B, the shock wave is caused by the wall wedge and is amplified by a strong shock coming from the PIMs. At the beginning of PIM operation, this shock impacts the heated near-wall fuel jets, thus enhancing the mixing processes.

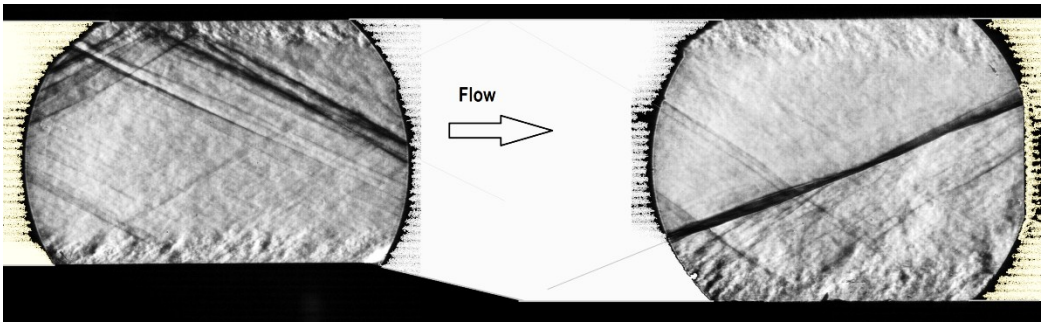

a.

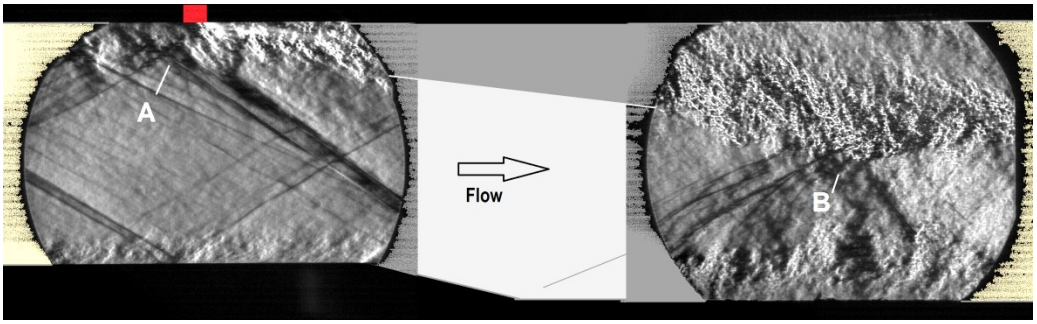

b.

Figure 9. Composite schlieren images illustrating the flow structure in test section. Each composite image consists of a pair of images taken through two different windows during different runs, combined into one. Black areas show the contour of combustor walls, red rectangle indicates the PIM location. (a) No fuel injection, discharge is turned on, I_{pl}= 4 A; (b) Ethylene injection mass flow rate G_{C2H4}= 3 g/s, the extent of the wedge-like combustion zone between the two windows is interpolated in gray color. Labels A and B indicate regions of potential development of Richtmyer-Meshkov instability.

Pressure distributions measured along the test section are plotted in Fig. 10 vs. fuel mass flow rate, used as a parameter, for two values of average discharge current, I_{pl}= 4 A and 2 A. The reduction of the discharge power between these two series of cases is only about 25%. It can be seen that operation with discharge turned on but without fuel injection does not affect the baseline pressure profile measured without the discharge, except for a small region located downstream of the electrodes (compare traces labeled “Flow” and “Dis” in Fig. 10). The effect of fuel injection, without the discharge, is also negligible compared to pressure rise caused by combustion. At sufficiently high values of discharge power and fuel injection mass flow rate, a significant increase of wall pressure is observed over a wide range of fuel flow rates, as shown in Fig. 10(a). In lean mixtures, ignition is detected downstream, as far as X>250 mm from the location of the plasma / airflow / fuel injection interaction region (note that this is not visible in the schlieren images). Measurements of the pressure distribution without fuel injection demonstrate that this zone is affected first by an expansion wave (detected by sensors at X=150-200 mm), and later by a strong compression wave caused by the angle expansion on the bottom wall. Shock-induced boundary layer separation may well occur in this region, which is likely to induce ignition due to long flow residence time. As the fuel injection flow rate is increased, the flame front moves forward and gradually occupies the entire combustor downstream the injector location. Operating at fuel mass flow rate above $G_{C2H4} \approx 6$ g/s may lead to thermal chocking in this combustor geometry. Increasing the duct expansion angle may resolve this difficulty.

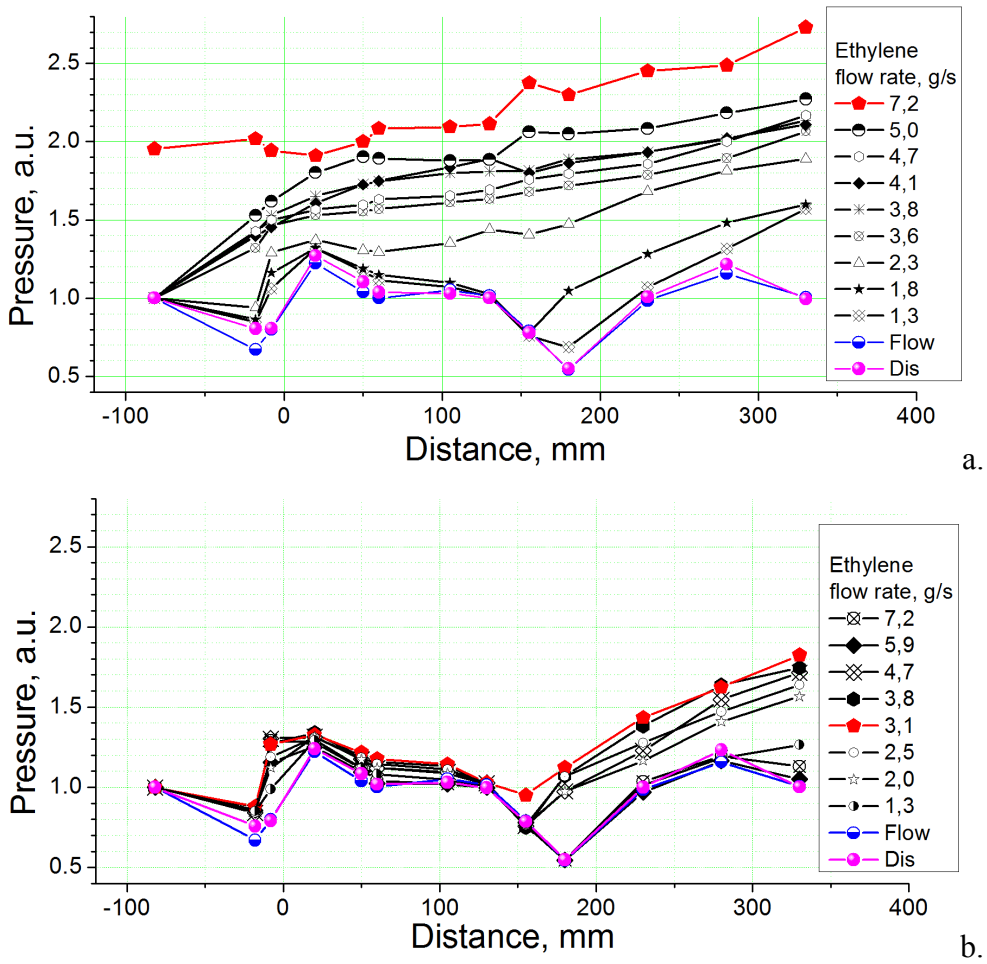

Figure 10. Normalized pressure P/P_{st}(X=-82 mm) profiles along the combustor vs. fuel mass flow rate: (a) Mode A, average current I_{pl}= 4 A, total discharge power W_{Σ}= 16-18 kW; (b) Mode A, I_{pl}=2 A, W_{Σ}= 12-14 kW. Numbers in the legend indicate ethylene mass flow rate G_{C2H4} in g/s; points labeled "Flow" taken without fuel injection, with the discharge turned off; points labeled "Dis" taken without fuel injection, with the discharge turned on.

Similar processes were detected in a lower-power discharge, over a narrow range of fuel injection rates, as shown in Fig. 10(b). At low fuel injection rates, ignition is detected far downstream of the injectors. As the fuel injection flow rate is increased, the pressure begins to increase but only to a certain limit, until the pressure rise levels off at $G_{C2H4} \approx 3$g/s, in contrast with the previous cases shown in Fig. 10(a). Further increase of fuel injection flow rate actually begins to inhibit combustion. The rarefaction wave, originating in the duct extension, reduces the pressure and, therefore, the rate of chemical reactions in the region located upstream (x=150-180 mm) of shock-promoted ignition zone (x=180-220 mm). In this case, the discharge power appears to be insufficient for the flame front to propagate across this low-pressure region. In

addition to reduction of heating by the discharge (by about 25%), two effects may be responsible for this: (a) insufficient fuel activation by the discharge, and (b) insufficient fuel-air mixing enhanced by the plasma. Numerical modeling [30], included plasma-chemical kinetics and mixing processes, indicates that the second effect may be dominant.

The results of the last series of experiments show that reducing the power in each plasma module is not necessarily beneficial for optimizing the power budget, due to existence of discharge power threshold required to accomplish stable flameholding.

4.2. Pressure dynamics depending on PIM's mode.

Typical wall pressure traces taken during supersonic combustion of ethylene are shown in Fig. 11, for different discharge operation modes. During operation in Mode A, when all PIMs were powered, reproducible ignition and stable combustion have been observed, as shown in Fig. 9(a). It can be seen that the wall pressure increases at all axial locations along the combustor, downstream from the injection ports. At G_{C2H4}>3g/s, pressure rise is also detected upstream of the fuel injectors, which is explained by flow separation near the side walls. After beginning of injection, ignition is first detected far downstream of the injector ports, and subsequently the flame front rapidly propagates upstream. The process of combustion stabilization (i.e. reaching steady-state flameholding) takes no longer than $\tau_{FH} < 20$ ms after the start of fuel injection. Most likely, flame propagation occurs along the top corners of the duct, with simultaneous development of flow separation in the side zones.

During operation in Mode B, with the lateral plasma modules turned off, the total discharge power is reduced to about 60% of that in Mode A, when all four modules are powered. At these conditions, if the fuel injection rate is outside of the optimal range of G_{C2H4}=3.0-4.5 g/s, the test section pressure is significantly lower compared to Mode A. At near optimal operating conditions, the pressure measured for Mode B is close to the one for Mode A. Another significant difference of Mode B from Mode A is slower flame stabilization, $\tau_{FH} > 40$ ms. In Mode C, the effect of side walls prevents formation of an extended combustion zone. The present hypothesis is that flow separation in the corners of the duct leads to the mixture being too fuel-rich in the separation zones. Because of this, operation in Mode C was excluded from further testing and analysis. In Mode D only a single, centrally located, plasma module is powered, producing ignition at fuel-rich conditions but unable to stabilize the flame front. Strong pressure oscillations were observed in the test section in this case. At lower fuel mass flow rates, weak combustion was detected far downstream of the injection port, X > 250 mm.

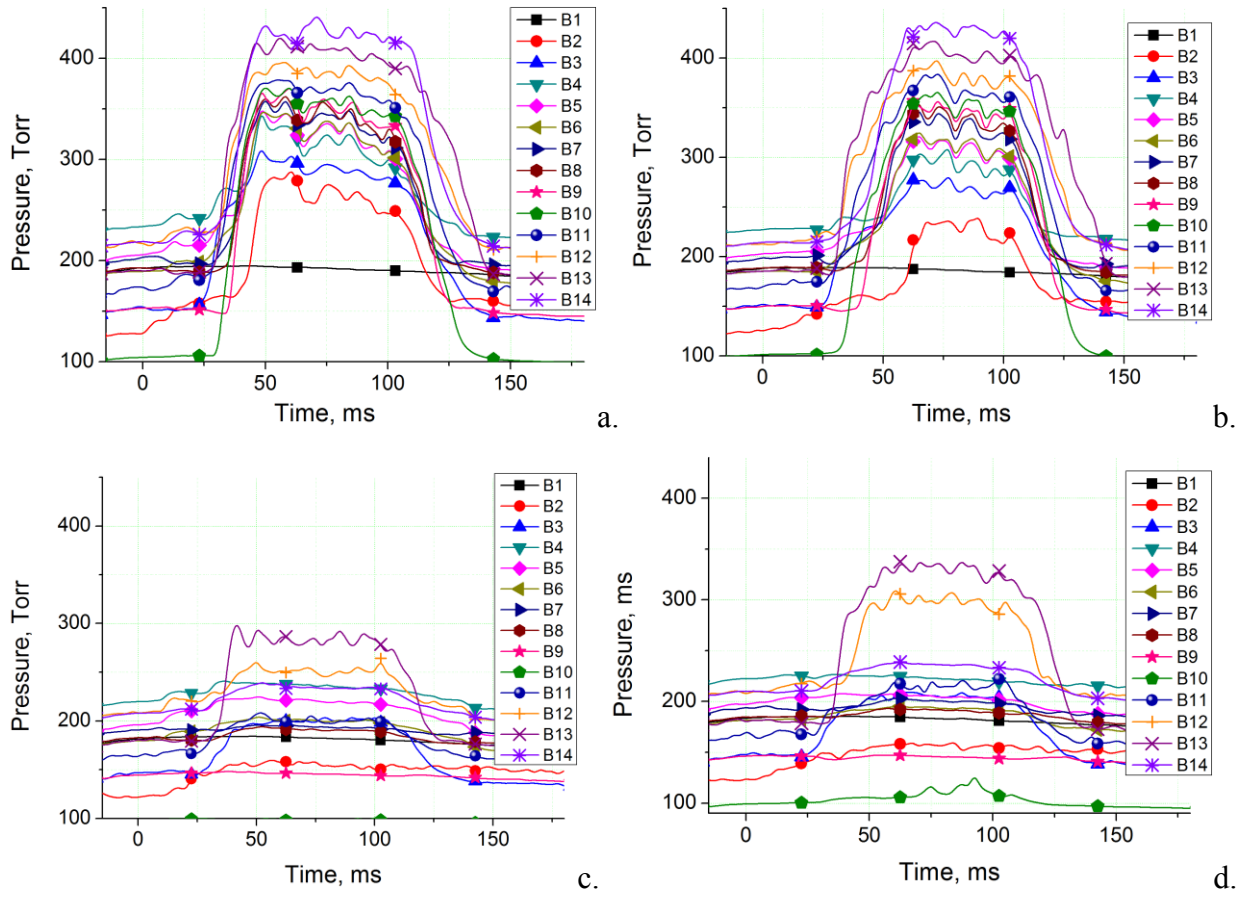

Figure 11. Typical pressure traces during supersonic combustion of ethylene: (a) Mode A; (b) Mode B; (c) Mode C; (d) Mode D. G_{C2H4}= 3.6 g/s; average discharge current I_{pl}= 4 A.

Additional tests were performed to study the effect of the number of plasma modules powered on wall pressure rise vs. fuel flow rate. The results are presented in Fig. 12, for two selected axial locations in the test section, X=60 mm from the PIM modules (Fig. 12(a)) and X=230 mm (near the initial ignition location, Fig.12(b)). Mode A (all four plasma modules are powered) demonstrates the best performance among the three operation modes tested in terms of wall pressure rise. Mode B (two plasma modules are powered) exhibits similar performance to Mode A at low fuel injection flow rates. It is apparent that Mode D (only one plasma module powered) cannot compete with the first two operation modes within the range of parameters tested. It should be noted that there is a range of fuel mass flow rates where Mode B becomes nearly saturated in terms of pressure rise vs. fuel injection rate, beginning at $G_{C2H4} \approx 4$g/s. Mode A exhibits similar behavior near this value of fuel feeding. This effect corresponds to combustion instability development.

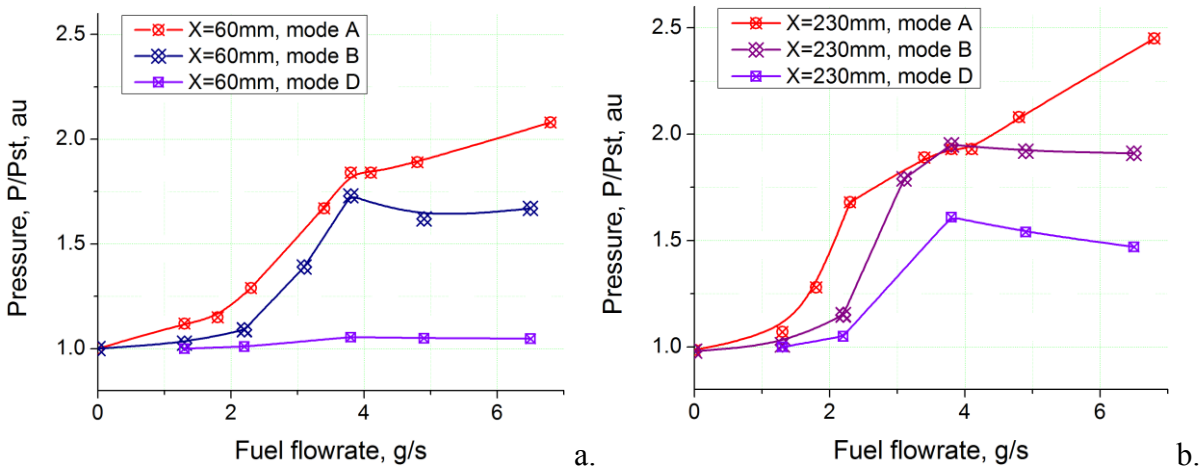

Figure 12. Relative pressure at two selected locations of the combustor vs. fuel mass flow rate. I_{pl}= 4A; (a) X=60 mm; (b) X=230 mm.

4.3. Combustion instability development

Along with insufficient mixing, the second formidable problem for effective plasma-based flameholding is large-scale combustion instability (periodic receding of the flame front). This results in strong variation of electric discharge power and combustor pressure, rapid modification of the flow structure, and disastrous mechanical vibrations of the facility. Figures 13 and 14 illustrate some of the features of this phenomenon. Figure 13(a) compares discharge power dynamics for different discharge operation modes and fuel mass flow rates. Typically, the oscillations appear earlier and have higher amplitude at higher discharge powers and during more intense combustion (i.e. at higher fuel flow rates). The phases of discharge voltage and pressure oscillations are strongly coupled, as is apparent from Fig. 13(b). The instability process starts from a pressure rise, followed by a voltage drop and resulting in pressure reduction. This behavior suggests the following mechanism of oscillations: intense combustion at fuel-rich conditions leads to pressure (P) elevation, causing flow separation in the duct and movement of the separation zone upstream, as shown in frames 1, 2, and 3 of Fig. 14. When the separation zone reaches the plasma modules, the discharge filament, previously extended by the flow (see discussion in Section 3 and Fig. 8(b)), becomes much shorter and terminates near the fuel injection orifice. Additionally, in a low-speed flow separation region, gas temperature in the plasma filament (T_g) increases, gas density (ρ) decreases, and electrical conductivity (σ) rises. The combination of the two factors, (a) discharge filament length (L) reduction, and (b) conductivity rise, results in significant drop of discharge voltage (U_{pl}) and discharge power (W_{pl}).

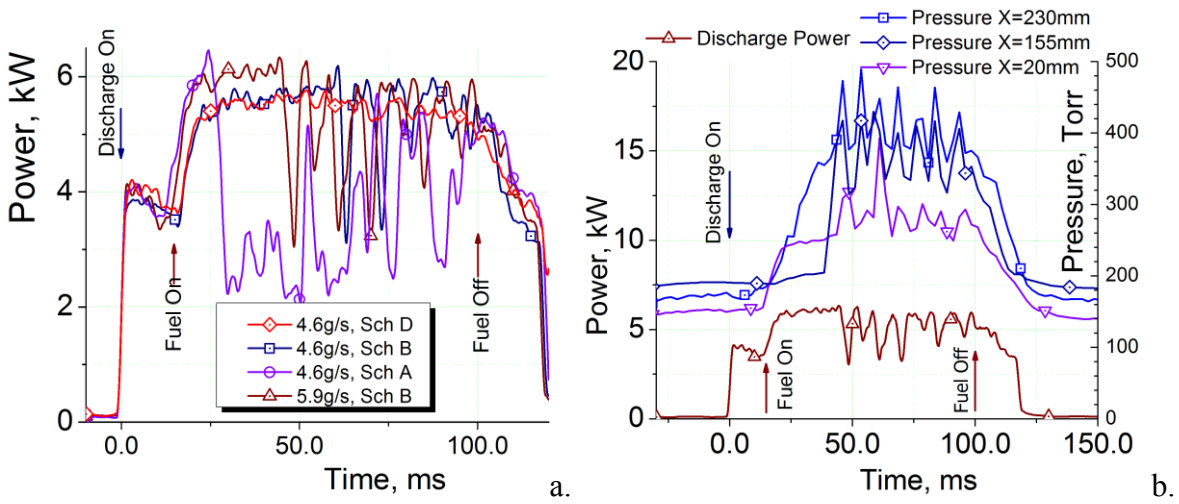

Figure 13. (a) Discharge power trace, and (b) wall pressure traces illustrating combustion instability at a high fuel injection flow rate, G_{C2H4}=5.9g/s. The power shown is for PIM #3, average discharge current I_{pl} = 4 A, low-pass cutoff filter is applied.

Since at these conditions the plasma is no longer able to support combustion, chemical power release (Q_{com}) is sharply reduced, resulting in gradual restoration of the baseline flow structure, as shown in schlieren images 4, 5, and 6 in Fig. 14. The instability feedback loop is closed due to combustion extinction limit being sensitive to the discharge power, as illustrated in the diagram in Fig.15. Passive or active control of the electric discharge parameters, as well as optimization of duct wall profile, may well be able to delay the onset of this instability or suppress it entirely.

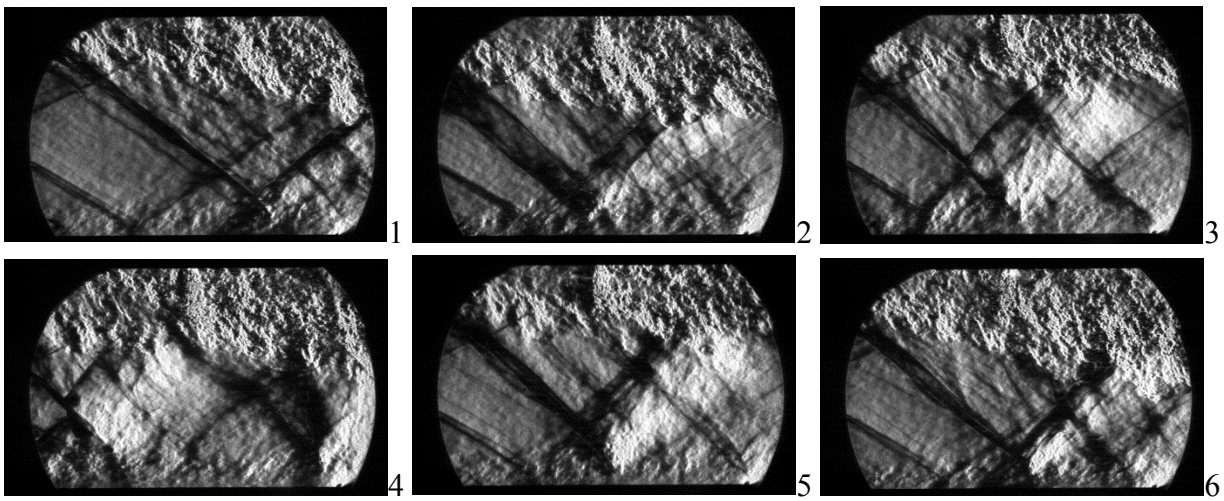

Figure 14. A series of schlieren images for a single oscillation cycle in the combustor, taken through the upstream pair of windows. Flow direction is from left to right. PIMs are located on the top wall, discharge operates in Mode A, G_{C2H4}=6.5 g/s, I_{pl}=4 A, time interval between the frames is 2 ms, the frames are labeled in order.

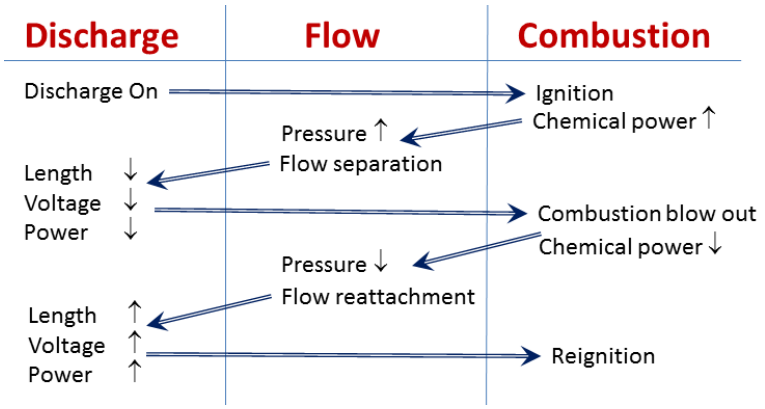

Figure 15. Diagram illustrating a feedback loop of combustion instability development. Small vertical arrows show an increase (up) or reduction (down) of parameter values. Larger inclined arrows show the sequence of processes involved.

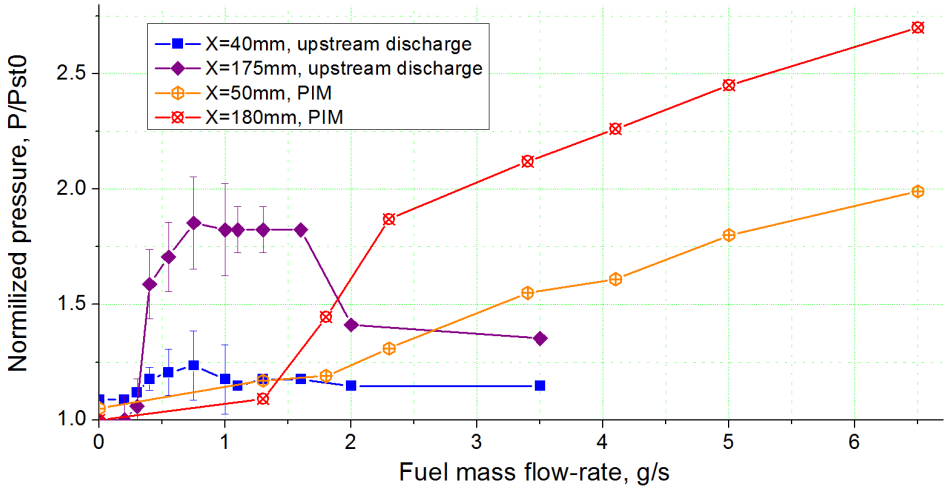

Figure 16. Comparison of the present data to previous results, obtained for the configuration with discharge generation upstream of the fuel injector [11]. Flow parameters (M=2, P_{st}=180-200Torr) and discharge power (W_{pl}=12-18 kW) are similar in both cases, axial location X is measured from the row of electrodes.

Figure 16 demonstrates a striking difference between the performance of two different schemes applied for plasma-based ignition and flameholding: the previously used scheme with plasma generation upstream of the fuel injection port [10, 11, 20], and the present scheme with collocated plasma generation and fuel injection, combined to a single unit. The previously used scheme exhibits more effective ignition at fuel-lean condition, i.e. at low fuel flow rates. The present configuration, however, shows much better performance at fuel-rich conditions, where

the previous scheme is limited to partial oxidation with fairly insignificant increase of pressure. Lean combustion limit for the present configuration is G > 1 g/s, while for the previous scheme it was G < 0.4 g/s. In the present experiments, increasing the ethylene flow rate results in more pronounced pressure rise (i.e. in more intense combustion), which was not the case for previously tested configurations. To interpret this difference, two key points need to be made: (1) in the old scheme, the discharge was sustained in air, while in the present scheme it is sustained in the fuel (inside the injection orifice) as well as in the fuel-air mixture; and (2) the flow structure in the present configuration is significantly different. Specifically, near-surface quasi-DC discharge used in the previous scheme [11] produces a "closed" flow separation zone (a separation bubble) downstream of the discharge, with high concentrations of chemically active species, such as atomic oxygen (O) and electronically / vibrationally excited nitrogen (N_2^*). The fuel, after being injected into this zone, has sufficiently long residence time to mix with plasma-activated air and ignite. After ignition, the volume of this zone increases and forms an extended subsonic flow zone without obvious reattachment downstream. Further increase of fuel mass flow rate results in extremely fuel-rich conditions in the separation zone, with subsequent flame extinction / blow-off. At these conditions, residual pressure increase indicates partial oxidation of fuel by active species generated by the discharge. In contrast to this pattern, in the new scheme the discharge is localized along the fuel injection jet, which generates reactive species and radicals, such as H, CH, C_2H_3, etc., by electron impact, and enhances mixing by convecting the discharge filament with the injection jet (as discussed in Section 3). Based on the present results, it appears that filament convection with the flow becomes significant only at sufficiently high fuel injection speed, comparable with the main airflow velocity. This explains why ignition at fuel-lean conditions is not observed (see Fig. 15).

5. Conclusions

Significant progress in plasma-assisted supersonic combustion and flameholding has been achieved at a high-speed combustion facility PWT-50H, using flush-mounted installation of discharge modules. The use of this method may potentially lead to reduction of total pressure losses when operating the combustor under non-optimal conditions, enhancement of operation stability and, consequently, expanding the air-breathing corridor of scramjet operation range. The concept of plasma-assisted combustion includes not only accelerating ignition, but also mixing enhancement when operating at non-premixed conditions, and flame stabilization (flameholding). This paper presents experimental results exhibiting significant performance enhancement based on new mechanisms of plasma-flow interaction, which have not been understood previously.

The present work discusses a novel scheme of a combined electric discharge / fuel injection module, with the high-voltage electrode placed inside the fuel injection orifice. After breakdown is achieved, the discharge current path follows the fuel injection jet due to lower gas density in the jet and convective entrainment of the plasma by the flow. The axial part of the

plasma filament is localized inside the fuel-air mixing layer. The plasma filaments are extended by the fuel injection flow, penetrate into the main airflow, and terminate far downstream, at the edge of ceramic insert plates, which is critically important for fuel-air mixing enhancement. To the best of our knowledge, this approach (specifically involving plasma generation in the fuel injection jet) has not been used previously for high-speed combustion enhancement.

Using this approach, stable flameholding has been observed over a wide range of fuel injection mass flow rates. Four discharge modules are installed in the supersonic combustor to study their capability for ignition and flameholding. Critical importance of plasma module and combustor geometry, as well as of key operation parameters such as total discharge power, W_{pl}> 5 kW for each module, and fuel mass flow rate, G_{C2H4}>1g/s, has been demonstrated. Development of large-scale combustion instability is identified as the limiting mechanism of plasma-based flameholding in the present configuration. On the other hand, the present experiments illustrate possible ways for further improvement of this technique, including the use of contoured injector orifices for supersonic injection and a power supply with a modified voltage-current characteristic. Finally, the new scheme demonstrates a significant advantage in terms of flameholding limits, compared to previously tested configurations.

Acknowledgments

This work has been supported by AFOSR (contract monitor: Dr. Chiping Li) and AFRL (contract monitor: Dr. Campbell Carter).

Appendix

In a non-electronegative plasma, discharge behavior during cross-flow fuel injection can be quantified using a plasma fluid model, incorporating equations for electron and ion densities and the Poisson equation for the electric field, listed below for non-electronegative plasma:

$$\frac{\partial n_e}{\partial t} + \nabla\left(-D_e \nabla n_e - \mu_e n_e \vec{E} + n_e \vec{u}\right) = \nu_{ion} n_e - \beta_{ei} n_i n_e \quad , \tag{1}$$

$$\frac{\partial n_i}{\partial t} + \nabla\left(-D_i \nabla n_i + \mu_i n_i \vec{E} + n_i \vec{u}\right) = \nu_{ion} n_e - \beta_{ei} n_i n_e \quad , \tag{2}$$

$$\nabla \vec{E} = \frac{e}{\varepsilon_0}(n_i - n_e) \quad . \tag{3}$$

In Eqs. (1-3), n_e and n_i are electron and ion densities, D_e and D_i are their diffusion coefficients, μ_e and μ_i are the mobilities, $\vec{E}$ is the electric field, $\vec{u}$ is the flow velocity, $\nu_{ion}(E/N)$ is the electron impact ionization frequency, N is the number density, and β_{ei} is the electron-ion recombination coefficient. Eqs. (1-3) are valid on the time scale longer than electron-neutral and ion-neutral collision frequencies, $\tau >> \max\left\{[N\nu_e(T_e)\sigma_{en}]^{-1}, [N\nu_i(T)\sigma_{in}]^{-1}\right\}$, where v_e and v_i are electron and ion thermal velocities, T_e is the electron temperature, and σ_{en} and σ_{in} are electron-neutral and ion-neutral collision cross sections.

The plasma model needs to be coupled with Navier-Stokes flow equations, predicting velocity, temperature, and species concentrations in non-premixed, reacting, compressible fuel-air flow (e.g. see the problem formulation for supersonic airflow in Ref. [29]), as well as electron energy equation. The fuel-air chemistry reaction set also needs to incorporate plasmachemical reactions [30]. However, a simple qualitative estimate can be obtained on the spatial scale (filament diameter) much larger than the Debye length, $L >> d = (\varepsilon_0 k T_e / e^2 n_e)^2$, $L \sim 0.1$ cm, $d \sim 10^{-4}$ cm at the present conditions ($T_e \sim 1$ eV, $n_e \sim (4 \div 5) \times 10^{15}$ cm^{-3}), such that the plasma is quasi-neutral, $n_e \sim n_i \sim n$, and its behavior in the flow is described by a single equation,

$$\frac{\partial n}{\partial t} + \nabla\left(-D_a \nabla n\right) + \vec{u}\nabla n = \nu_{ion} n - \beta_{ei} n^2 \quad , \tag{4}$$

where $D_a \sim 5 \cdot 10^3 \cdot T_e$ [eV] / P [Torr] cm^2/s [31] is the ambipolar diffusion coefficient. Eq. (4) assumes steady incompressible flow, such that $\nabla \vec{u} = 0$. For flow velocities greater than $u \sim D_a / L \sim$ 5 m/s, ambipolar diffusion in Eq. (4) can be neglected. Since at the present conditions $\nu_{ion} \sim \beta_{ei} n \sim 10^7$ s^{-1} >> $u/L \sim 3 \cdot 10^5$ s^{-1} (i.e. local ionization balance is maintained), Eq. (4) becomes

$$\frac{\partial n}{\partial t} + \vec{u}\nabla n \approx 0 \quad , \tag{5}$$

which has a steady-state solution only if

$$\vec{u} \perp \nabla n \, , \tag{6}$$

i.e. if the direction of the plasma filament (perpendicular to ∇n) is parallel to the velocity vector, which is the sum of the main flow velocity and the injection flow velocity, $\vec{u} = \vec{u}_{air} + \vec{u}_{fuel}$. If this condition is not satisfied, a self-similar transient solution is realized,

$$\frac{dn}{d\vec{\xi}} \approx 0, \quad n(\vec{\xi}) = n(\vec{r} + \vec{u}t) = const \quad , \tag{7}$$

i.e. the plasma (the electrons and the ions together) will be convected with the flow, in the direction of the velocity vector $\vec{u}$.

Thus, at the present conditions, the near-steady-state plasma filament essentially follows the velocity vector of fuel injection jet as it is gradually mixing with the main flow, according to Eq. (6), penetrating into the main flow a few mm away from the wall (see Fig. 8(b)). Since the discharge current follows the plasma filament, $\vec{j} \perp \nabla n$, the current is parallel to the flow velocity vector, $\vec{j} \parallel \vec{u}$. This shows that filament displacement by the flow extends the electric field region into the main flow, $\vec{E} \approx \vec{j} / \mu_e n - (kT_e / e)\nabla n / n$ [31]. The second term in this equation (the field transverse to the filament) appears if ambipolar diffusion is not neglected in Eq. (4). In the absence of fuel injection, on the other hand, the filament follows the shortest path between the electrodes, parallel to the main flow velocity vector. Convection of the plasma by the flow dominates until transverse "shortcut" electric field (between two pin electrodes [24], or between the filament and the grounded wall at the present conditions) becomes higher compared to the field along the filament. This may result in unsteady, repetitive discharge behavior [25].

Note that if the plasma density is fairly low, $\nu_{ion} \sim \beta_{ei} n \sim u / L$, such that local ionization balance in the flow is no longer maintained, the flow would result in spreading the plasma filament over a spatial scale L. For $L \sim 0.1$-1 cm and $u \sim 300$ m/s, the plasma density needs to be $n \sim u / \beta_{ei} L \sim 10^{13} - 10^{12}$ cm^{-3}, much lower than at the present conditions. This estimate is consistent with the results of kinetic modeling calculations [29] using Eqs. (1-3) coupled with compressible Navier-Stokes equations. A quantitative prediction of the current path requires using a self-consistent plasma / flow kinetic model, such as described above.

References

1. E.T. Curran - Scramjet engines: the first forty years // J. Propul. Power 17 (6), (2001) 1138–1148.
2. J. C. B. MacKeand - Sparks and Flames: Ignition in Engines : An Historical Approach, Tyndar Press, 1997
3. A. Starikovskiy, N. Aleksandrov - Plasma-assisted ignition and combustion // Progress in Energy and Combustion Science, Volume 39, Issue 1, February 2013, Pages 61–110
4. I.V. Adamovich, I. Choi, N. Jiang, J.-H Kim, S. Keshav, W.R. Lempert, E. Mintusov, M. Nishihara, M. Samimy, and M. Uddi - Plasma Assisted Ignition and High-Speed Flow Control: Non-Thermal and Thermal Effects // Plasma Sources Science and Technology, vol. 18, 2009, p. 034018
5. M.C. Billingsley, W.F. O'Brien, J.A. Schetz - Plasma torch atomizer-igniter for supersonic combustion of liquid hydrocarbon fuels // AIAA Paper 2006-7970.
6. H. Do, M.A. Cappelli, M.G. Mungal - Plasma assisted cavity flame ignition in supersonic flows // Combust. Flame 157 (9) (2010) 1783–1794.
7. L.S. Jacobsen, C.D. Carter, T.A. Jackson, et al. - Plasma-assisted ignition in scramjets // J. Propul. Power 24 (4) (2008) 641–654.
8. K. Takita, K. Shishido, K. Kurumada - Ignition in a supersonic flow by a plasma jet of mixed feedstock including CH4 // Proc. Combust. Inst. 33 (2) (2011) 2383–2389.
9. Fei Li, Xi-long Yua, Ying-gang Tong, Yan Shen, Jian Chen, Li-hong Chen, Xin-yu Chang - Plasma-assisted ignition for a kerosene fueled scramjet at Mach 1.8 // Aerospace Science and Technology 28 (2013) 72–78
10. S. Leonov, D. Yarantsev, V. Sabelnikov - Electrically Driven Combustion near the plane wall in a supersonic duct // Progress in Propulsion Physics, Advances in Aerospace Science, EUCASS book series, Vol 2, 2011, pp. 519-530
11. S. Leonov, C. Carter, D. Yarantsev - Experiments on Electrically Controlled Flameholding on a Plane Wall in Supersonic Airflow // Journal of Propulsion and Power, 2009, vol.25, no.2, pp.289-298
12. Z. Yin, I.V. Adamovich, and W.R. Lempert, "OH Radical and Temperature Measurements During Ignition of H2-Air Mixtures Excited by a Repetitively Pulsed Nanosecond Discharge", Proceedings of the Combustion Institute, vol. 34, 2013, pp. 3249–3258
13. S.M. Starikovskaia "Plasma assisted ignition and combustion," J. Phys.D: Applied Physics, 2006, vol.39, R265-R299.
14. W Sun, M Uddi, T Ombrello, SH Won, C Carter, Y Ju, Effects of non-equilibrium plasma discharge on counterflow diffusion flame extinction, Proceedings of the Combustion Institute 33 (2), 3211-3218, 2011
15. I N Kosarev, V I Khorunzhenko, E I Mintoussov, P N Sagulenko, N A Popov, S M Starikovskaia, A nanosecond surface dielectric barrier discharge at elevated pressures: time-resolved electric field and efficiency of initiation of combustion, - Plasma Sources Science & Technology, vol. 21, no. 4, 2012
16. V. Petrishchev, S. Leonov, and I. Adamovich, "Studies of Nanosecond Pulse Surface Ionization Wave Discharges over Solid and Liquid Dielectric Surfaces", Plasma Sources Science & Technology, 2014, submitted for publication.
17. Z. Xiong, E. Robert, V. Sarron, J-M. Pouvesle and M. Kushner, "Dynamics of ionization wave splitting and merging of atmospheric-pressure plasmas in branched dielectric tubes and channels", 2012 J. Phys. D: Appl. Phys. 45 275201

18. V. A. Bityurin, A. N. Bocharov, and N. A. Popov, “Numerical Simulation of an Electric Discharge in Supersonic Flow”, Fluid Dynamics, 2008, Vol. 43, No. 4, pp. 642–653
19. S. B. Leonov, A. A. Firsov, Yu. I. Isaenkov et al. - Plasma-Based Fast Mixing and Ignition in Supersonic Flow // Paper AIAA 2011-2327
20. A. Firsov, Leonov S., Yarantsev D. et al - Temperature Measurement in Plasma-Assisted Combustor by TDLAS // Paper AIAA 2012-3181
21. C. O. Laux, T. G. Spence, C. H. Kruger and R. N. Zare, “Optical diagnostics of atmospheric pressure air plasmas”, Plasma Sources Sci. Technol. 12 (2003) 125–138
22. M. A Gigososy and V. Cardenosoz, “New plasma diagnosis tables of hydrogen Stark broadening including ion dynamics”, J. Phys. B: At. Mol. Opt. Phys. 29 (1996) 4795–4838.
23. H. R. Griem, “Stark Broadening of the Hydrogen Balmer-α Line in Low and High Density Plasmas“, Contrib. Plasma Phys. 40 (2000), pp.46-56
24. S. B. Leonov and D. A. Yarantsev, “Near-Surface Electrical Discharge in Supersonic Airflow: Properties and Flow Control”, Journal of Propulsion and Power, vol. 24, 2008, pp. 1168-1181
25. S.H. Zaidi, T. Smith, S. Macheret, and R.B. Miles, ”Snowplow Surface Discharge in Magnetic Field for High Speed Boundary Layer Control, AIAA Paper 2006-1006, 44th AIAA Aerospace Sciences Meeting and Exhibit, 9-12 January 2006, Reno, Nevada; C.S. Kalra, S.H. Zaidi, R.B. Miles, and S.O. Macheret, “Shockwave–turbulent boundary layer interaction control using magnetically driven surface discharges”, Experiments in Fluids, vol. 50, 2011, pp. 547–559
26. R.K. Janev and D. Reiter, “Collision Processes of C2,3Hy and C2,3Hy+ hydrocarbons with Electrons and Protons”, Physics of Plasmas, vol.11, 2004, pp. 781-829
27. M. A. Deminsky, I. V. Kochetov, A. P. Napartovich, S. B. Leonov, - “Modeling of Plasma Assisted Combustion in Premixed Supersonic Gas Flow”, International Journal of Hypersonics, Volume 1, N 4, December 2010, pp. 5-15
28. A. A. Zheltovodov and E. A. Pimonov, “Using a Localized Pulse Periodic Energy Supply for Intensification of Mixing of Parallel Compressible Flows”, Technical Physics Letters, 2013, Vol. 39, No. 11, pp. 1016–1018
29. V. A. Bityurin, A. N. Bocharov, and N. A. Popov, “Numerical Simulation of an Electric Discharge in Supersonic Flow”, Fluid Dynamics, 2008, Vol. 43, No. 4, pp. 642–653
30. Z. Yin, A. Montello, C.D. Carter, W.R. Lempert, and I.V. Adamovich, “Measurements of Temperature and Hydroxyl Radical Generation / Decay in Lean Fuel-Air Mixtures Excited by a Repetitively Pulsed Nanosecond Discharge”, Combustion and Flame, vol.160, 2013, 1594–1608
31. Yu. P. Raizer, Gas Discharge Physics (Springer-Verlag, Berlin, 1991)